Marine Pollution Bulletin 194 (2023) 115395

Contents lists available at ScienceDirect

Marine Pollution Bulletin

journal homepage: www.elsevier.com/locate/marpolbul

Retention of buoyant plastic in a well-mixed estuary due to tides, river discharge and winds

Zheng Chen *, Gaoyang Li, Melissa Bowen, Giovanni Coco

School of Environment, Faculty of Science, the University of Auckland, Auckland, New Zealand

ARTICLE INFO

Keywords:
Buoyant plastic retention
Numerical simulations
Well-mixed estuaries
Spring-neap tides
Retention of plastics after storm events
Lateral circulation

ABSTRACT

Estuaries can act as plastic retention hotspots, but the hydrodynamic controls on retention are not well understood. This study investigates the retention of river-sourced buoyant plastics in a well-mixed estuary, the Waitematā Estuary, using validated numerical simulations of floats with different tides, winds, and freshwater discharge. The proportion of floats grounded on the shore in all seven simulations is higher than 60 % and over 90 % in five simulations after ten days. <20 % of the floats leave the estuarine mouth in any of the simulations. An increase of two orders of magnitude in freshwater discharge doubles the likelihood for floats to reach the lower estuary. However, we find increased freshwater discharge doubles the lateral circulation towards the shore and results in similar proportions of grounding (90 %) as the low discharge cases. These findings challenge the conventional view that plastics preferentially enter the open ocean after high river discharge.

1. Introduction

While international concerns over mismanaged plastic pollution causing enduring ecological degradation and socio-economic loss are increasing (Andrady, 2011; Wilcox et al., 2015; Lebreton et al., 2017; Blettler et al., 2018; Thiel et al., 2018; Hong et al., 2017; Honingh et al., 2020; Mcllgorm et al., 2020), the understanding of the transport and fate of plastic is still limited (Krelling and Turra, 2019; Meijer et al., 2021; Pinheiro et al., 2021). Although rivers and estuaries are considered the source of marine plastics (Lebreton et al., 2017; Thompson, 2015; Lima et al., 2020), recent observational (van Emmerik et al., 2019a; Tramoy et al., 2020a; Newbould et al., 2021; Ryan and Perold, 2021) and results from simulations (Mai et al., 2020; Bellasi et al., 2020; Meijer et al., 2021) support the hypothesis that most land-based plastics do not simply reach the ocean (van Emmerik et al., 2022a), but are instead partially retained in estuarine systems (Vermeiren et al., 2016; van Emmerik et al., 2020; Tramoy et al., 2020b; Chen et al., 2022; Cardoso-Mohedano et al., 2023). This near-shore retention is a leading explanation for why the previous riverine plastic input is an overestimate of the amount in the open ocean (Van Sebille et al., 2020) based on global annual production and disposal (Lebreton et al., 2017; Schmidt et al., 2017). In fact, the role of estuaries in regulating the amount of plastic entering the ocean has been understudied and further investigation of key mechanisms in estuarine plastic transport and retention are needed (Vermeiren et al., 2016).

The retention and transport mechanisms of river-sourced plastics in estuaries are complex and spatio-temporally dependent (Vermeiren et al., 2016; Zhang, 2017). Some mechanisms of transporting plastics in rivers have been studied using observations and numerical simulations (Balas et al., 2001; Tramoy et al., 2019) and some studies have considered the nearshore ocean dynamics (Van Sebille et al., 2012; Collins and Hermes, 2019). However, the mechanisms of transporting plastic in an estuary remain largely unknown (Duncan et al., 2020; van Emmerik et al., 2019a). Simulating the transport of plastic due to the tides, wind, river flows and the response to morphological features in an estuary requires validation (Zhang, 2017; Atwood et al., 2019; Ryan and Perold, 2021) but observational data are often insufficient at the local scale (van Emmerik and Schwarz, 2020; Duncan et al., 2020; Vermeiren et al., 2016). The recent development of remote sensing (Martínez-Vicente et al., 2019), GPS drifter trackers (Tramoy et al., 2020a) and beach clean-ups (Andrady, 2017) should provide more observational data in future at the local scale. Recently, high-resolution numerical simulations become a more common tool to explore the transport of plastics in complex estuarine settings (Gérigny et al., 2022; Lemagie and Lerczak, 2015).

Plastic transport and retention are not well linked with hydrodynamic mechanisms in all types of estuaries. Observations in river-dominated estuaries (for example, Seine River by van Emmerik et al.,

* Corresponding author.
E-mail address: zche440@aucklanduni.ac.nz (Z. Chen).

https://doi.org/10.1016/j.marpolbul.2023.115395
Received 7 March 2023; Received in revised form 4 August 2023; Accepted 5 August 2023
Available online 26 August 2023

2019b; Paranagua Estuary by Krelling and Turra, 2019; Saigon River by Schreyers et al., 2023; and Rhine River by van Emmerik et al., 2022b) all find that high river discharge enhances the downstream transport of plastics, potentially flushing more plastics into the ocean. The effects of tides and winds on plastic transport are more complicated (Blondel and Buschman, 2022). For example, the bidirectional tidal currents limit downstream transport and enhance the retention of plastics at the mouth (Schreyers et al., 2023; van Emmerik et al., 2022b). Most of the studies to date have been conducted in river-dominated systems consisting of long rivers with large discharge (van Emmerik et al., 2019b). Urban centres generating plastic pollution are also located in other types of estuaries, such as tidally-dominant estuaries with short creeks. Here we examine the Waitematā Estuary, New Zealand, which is a short (15 km in length), tidally-dominant (spring tidal current amplitude of 1 ms^{-1}) estuary with much lower river discharge (annual average freshwater discharge of 5 m^3s^{-1}; Chen and Bowen, 2020). Our study examines the sensitivity of plastic retention to the tides, river discharge and winds in this type of estuary and contrasts it with other systems to provide more comprehensive understanding of the transport and fate of plastics in different estuarine systems.

This study is based on the past observational studies of plastics in the Waitematā Estuary, which connect the freshwater sources, plastic deposition in the sediment and transport through the estuary. Plastic pollution has been quantified by an increasing number of observational studies in the Waitematā Estuary and this urbanized harbour is viewed as a plastic hotspot (Gregory, 1978; Young and Adams, 2010; Dikareva and Simon, 2019; Bridson et al., 2020; Hope et al., 2021; Chen et al., 2022). Microplastics have been found in nine freshwater streams (Dikareva and Simon, 2019) and are likely transported further downstream to the estuary. Plastics with different size, shape and polymer composition are the dominant litter found during the beach clean-ups around both upper and lower reaches of the Waitematā Estuary, especially near residential and industrial areas (Gregory, 1978). Plastics are also found deposited on the banks mixed with surface sediment (Hope et al., 2021; Bridson et al., 2020). The retention of plastic debris was investigated by Chen et al. (2022) using GPS tracked drifters: they find over 50 % of drifters are retained in the estuary after two tidal cycles with marked differences between spring and neap tides. However, the drifters only operated for two tidal cycles and the long-term fate of plastics in these types of estuaries remains to be investigated. Field observations are limited by logistic costs (Huhn et al., 2012) from covering a wide range of situations. Therefore, simulations are an effective way to test sensitivity to processes and connect plastic accumulation and distribution to hydrodynamic mechanisms.

In recent years, numerical studies of tracking buoyant plastics have been carried out worldwide. Gérigny et al. (2022) recently investigated how buoyant microplastics continuously released from hotspots along the Rhone River reach the coast and how wind-induced circulation and currents affect particle retention within coastal zones. Particle tracking models have also been applied to trace the source of retained plastic debris both by integrating float trajectories backwards in time to estimate potential sources of beached plastic debris in the Northeast Atlantic (Strand et al., 2021) and by calibrating the response of buoyant marine litter to wind drag (Pereiro et al., 2018). However, past studies have not systematically investigated the sensitivity of transport and retention of buoyant plastics to tides, freshwater and winds. Our current work will focus on tracking simulated floats in short, shallow, well-mixed estuaries, using the Waitematā Estuary as a case study. Seven scenarios with different combinations of tides, river flow and winds are considered in this study to better estimate the transport of plastic through the estuary into the open ocean and the magnitude of plastic retention within it. The response of residual circulation to the tides, freshwater and wind is contrasted between scenarios. The implications of the outcomes to other estuaries and future numerical work in the study area are discussed.

2. Methods

2.1. Site description

The Waitematā Estuary (Fig. 1) covers 80 km^2 area and is surrounded by the city of Auckland, New Zealand. It is classified as a well-mixed, drowned river valley (Hume, 2018) based on its geomorphological features of shallow basin, narrow mouth, complex shorelines and numerous arms formed by branching tidal creeks (Hume et al., 2007). The Waitematā Estuary is commercially and recreationally utilized as the main harbour of Auckland, connecting the inner Hauraki Gulf with upstream tidal creeks including Henderson Creek, Rangitopuni Creek, Lucas Creek and Whau River (Green and Hancock, 2012). These rivers are assumed to be sources of land-based plastics transported downstream by the freshwater flow (Dikareva and Simon, 2019). The strong tidal currents, along with the low freshwater flow, result in vertically well-mixed salinity in the main channel (Chen and Bowen, 2020; Chen et al., 2022). The tidal height and velocity are markedly semi-diurnal with fortnightly spring-neap patterns (1.8–2.6 m in tidal range), minor diurnal and monthly variation (Chen et al., 2022). The bathymetry of the Waitematā Estuary consists of a central channel with several deep holes surrounded by a wide basin as well as bays, sandy beaches, intertidal and subtidal mudflats covered by mangroves (Green and Hancock, 2012; Fig. 1b).

2.2. Hydrodynamic model configuration and validation

A three-dimensional hydrodynamic model is set up in the Regional Ocean Modelling System (ROMS; Shchepetkin and McWilliams, 2005; Wilkin et al., 2005). The model covers the whole extent of the Hauraki Gulf (Fig. 1a) with the grid resolution gradually increased from 625 m-by-625 m at the northeast corner of the domain to 25 m-by-25 m in the area of interest, the enclosed area of the Waitematā Estuary proper (Fig. 1b). The bathymetry data are combined from three sources: the tidal flats are delineated by the Auckland Council high-resolution LiDAR data; the deeper areas of the estuarine channel are digitized by Land Information New Zealand (LINZ); the rest in Hauraki Gulf is developed by National Institute of Water and Atmosphere (NIWA) digital-elevation-model (Mackay et al., 2012). The model simulates the wetting-and-drying of tidal flats using a critical water depth at 0.1 m and the model domain lying 2.35 m above the mean sea level (MSL) is marked as permanently dry. The key parameters of the model set up are listed in the supplementary information.

The model is initialised with zero elevation, zero momentum and a salinity field synthesised from the HYCOM dataset and shipboard measurements (main channel of the Waitematā Estuary by Chen and Bowen, 2020; the upper estuary by Williams, 1986). The tidal forcing data are extracted from the TPXO v9.0 dataset (Egbert and Erofeeva, 2002) at the north-eastern Hauraki Gulf. The model is ramped up for 10 days to spin-up the flows and salinity. After the ramp-up period, the atmospheric conditions and river flows are changed according to the specifics of the scenario. The atmospheric data (precipitation, relative humidity, atmospheric temperature, wind speed and direction) around the Waitematā Estuary are derived from stations in the Auckland Council Environmental Data Portal. The atmospheric data outside the estuary are derived from Cliflo (Cliflo, 2021) and ERA-5 (Hersbach et al., 2020). All atmospheric data are spatially interpolated to the model grid and hourly averaged. The river discharge rates of nine major rivers (Fig. 1b) are downloaded from Environmental Data Portal. (The time series of the forcing data are shown in Supplementary Fig. S1).

The surface salinity, along-channel salinity and surface velocity in the simulation are validated against the field observations including shipboard CTD transects, surface deployed CTDs and bottom-mounted ADCP measurements (details of the observations are in Chen et al., 2022). The model performance is quantitatively described by the predictive Model Skill (MS; Willmott, 1982; Warner et al., 2005):

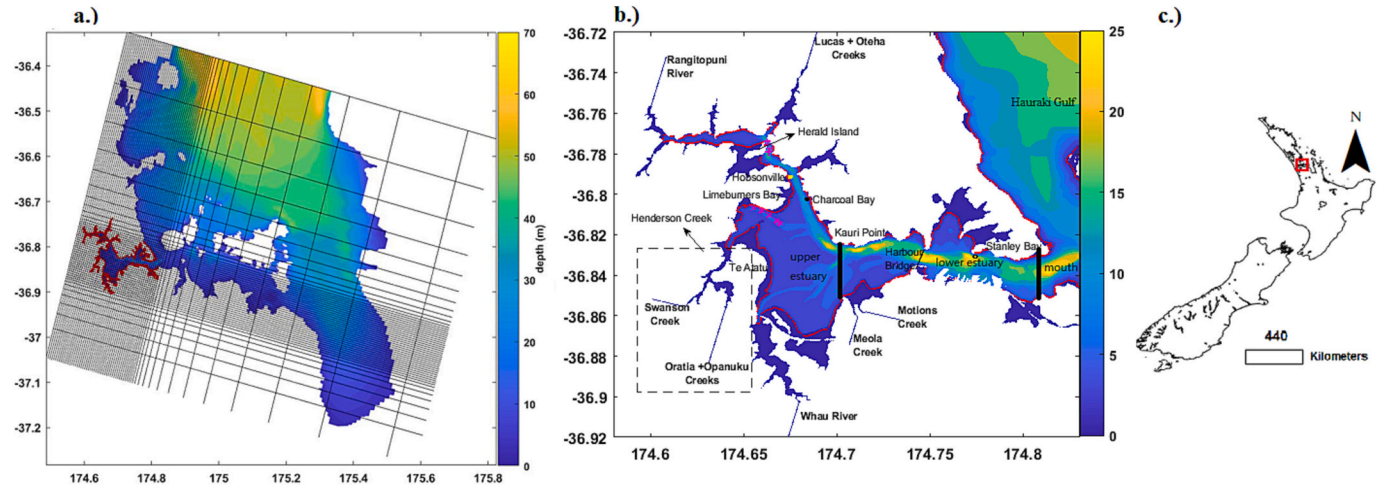

Fig. 1. (a) The model grid (cell boundaries in black lines) extends across the Hauraki Gulf and is chosen to finely resolve the estuary (red box). The bathymetry is shown by the colours with the scale in metres. (b) The Waitematā Estuary is shown in detail for the region inside the red box in (a). The bathymetry is shown by colours with the scale in metres. The red contour line delineates the boundary between the above-mean-sea-level tidal flats and the deeper part of the estuary; magenta crosses denote the launching locations of floats; freshwater sources have been indicated by bold text, while other important place names have also been annotated; yellow dots show the locations of two CTDs measuring surface salinity (Hobsonville, Stanley Bay) and black dots mark the locations of bottom-mounted ADCPs (Charcoal Bay, Stanley Bay). Two black lines mark the entrance of the lower estuary and the estuarine mouth. (c) The location of the Waitematā Estuary in New Zealand shown by the red box. (For interpretation of the references to colour in this figure legend, the reader is referred to the web version of this article.)

$$MS = 1 - \frac{\sum_{i=1}^{n}(X_{mdl} - X_{obs})^2}{\sum_{i=1}^{n}(|X_{mdl} - \overline{X_{obs}}| + |X_{obs} - \overline{X_{obs}}|)^2}$$

This metric is widely used in evaluating models including ROMS (Thyng et al., 2021; Haidvogel et al., 2008; Li et al., 2005). Based on the range of values reported in similar studies, MS over 0.80 is considered to show reasonable performance.

The flow velocity and salinity compare well with the field observations, which suggests the model can be used to simulate the hydrodynamics in the Waitematā Estuary. The modelled surface velocity matches moderately well with the ADCP measurements at Stanley Bay (MS = 0.79) and Charcoal Bay (MS = 0.81). The salinity measurements indicate better agreement at Hobsonville (MS = 0.82), the upper estuary, compared to the Stanley Bay (MS = 0.54; underestimated salinity). Nevertheless, the model results compare better with the observations at the larger scales: the along-channel salinity structure during the spring tide (MS = 0.97) is captured well in the simulation and the salinity transect during the neap tide also shows satisfactory performance (MS = 0.93; Details are given in the supplementary information S2).

2.3. Offline float tracking

For the aims of this sensitivity study, we have selected the offline Lagrangian tracking for its flexibility. Offline Lagrangian tracking computes the trajectories using the hydrodynamic model output (e.g., Van Sebille et al., 2018) and is more efficient compared to computing trajectories in the code alongside the hydrodynamics within the simulation. We developed an offline model in which virtual floats can be released at any time and location to investigate various situations using the surface velocities from the ROMS output. The floats remain at the surface and are moved according to the surface velocities. Floats have no windage but are impacted by the winds via the surface wind-driven circulation. The location of each float is calculated using a fourth-order Runge-Kutta numerical method (RK-4; equations in supplementary information) with horizontal velocities interpolated from four neighbouring grid cells at five-minute intervals. Floats ground when one of the neighbouring cells becomes dry: when a grid cell changes from wet to dry during ebbing tides, its corresponding surface velocity becomes undefined, and any float located adjacent to this grid cell becomes stationary. If the water level rises high enough to inundate grid cells and change their state to wet again, the float remobilizes and drifts following the interpolated surface flow velocity. An example of float trajectories is shown in Fig. 2.

2.4. Simulation scenarios

In each scenario, a total of 250 float trajectories are simulated. The floats are started at two locations, Herald Island (HI) and Henderson Creek (HC), the two main hypothesized sources of riverine plastics, in ten groups with 150 m separation between them. Within each group, 25 floats are started within 1.5 m of each other. The trajectory calculation starts at high slack tide in every scenario. This set-up is chosen to match the launching time and start positions of two field experiments where pairs of drifters were launched at 5 different locations in the two branches of the estuary during spring and neap tides (Chen et al., 2022). Float trajectories are computed for a total of ten days.

The model is run for seven scenarios, two baseline scenarios capturing the spring to neap (Baseline A) and neap to spring (Baseline B) tides (Fig. 3), and five additional scenarios that use the baseline tides but examine the sensitivity to freshwater and winds (Table 1). A pair of high river flow cases is run with a peak freshwater discharge of 300 m^3s^{-1}, typical of a 5-year event (Flow A and Flow B). Another pair of simulations (Wind A and Wind B) is run with the same baseline tides but with winds taken from wind observations during a storm event (wind speed up to 10 ms^{-1} in the lower estuary; Fig. 3). The last scenario (called "Actual Storm") uses a real severe event when the flood and storm damaged over 1000 properties in West Auckland (ICNZ, 2021). Compared to the baseline conditions, the wind speed (mainly easterlies) at the lower estuary is doubled and the peak freshwater discharge is increased by two orders of magnitude (Fig. 3). In late January 2023 after this study was complete, Auckland experienced another devastating flood followed two weeks later by the passage of a slow-moving tropical cyclone. Our storm simulation investigates how a severe event like this impacts the retention and transport of buoyant plastics and one which is very likely to reoccur in future.

2.5. Float statistics

The mobility of floats in different cases is evaluated using the computed float trajectories and calculating the proportion of floats

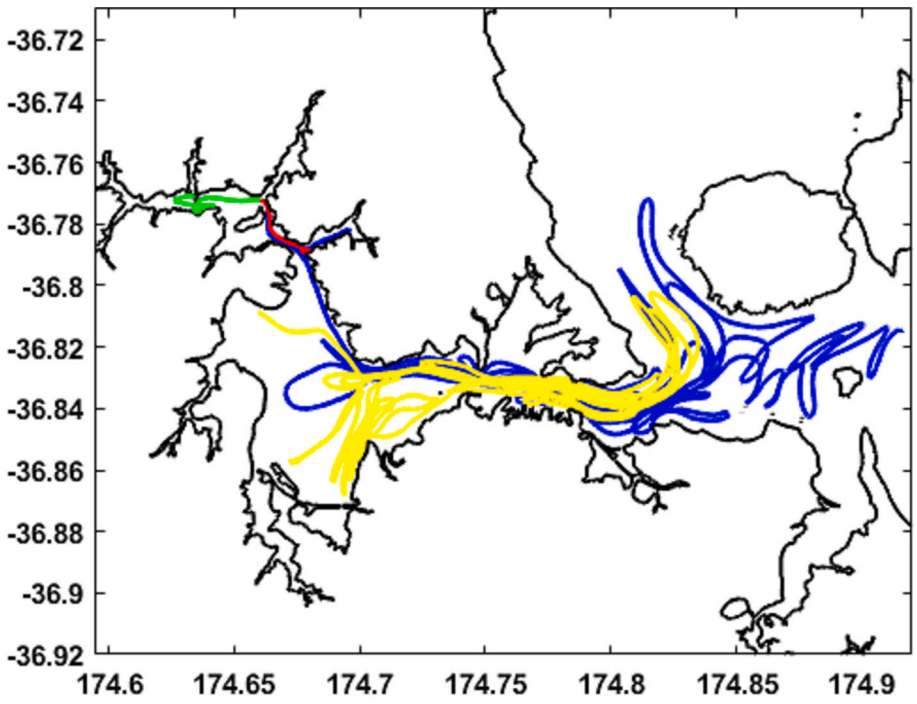

Fig. 2. Selected trajectories of floats during the simulation Baseline A show the range of possible behaviour: red shows a float launched from Herald Island that quickly grounds; Blue shows a float launched from Herald Island that exits the estuarine mouth and enters the Hauraki Gulf; Yellow shows a float launched from Henderson Creek that moves back and forth around the mouth; Green shows a float that moves upstream and grounds near Rangitopuni Creek. (For interpretation of the references to colour in this figure legend, the reader is referred to the web version of this article.)

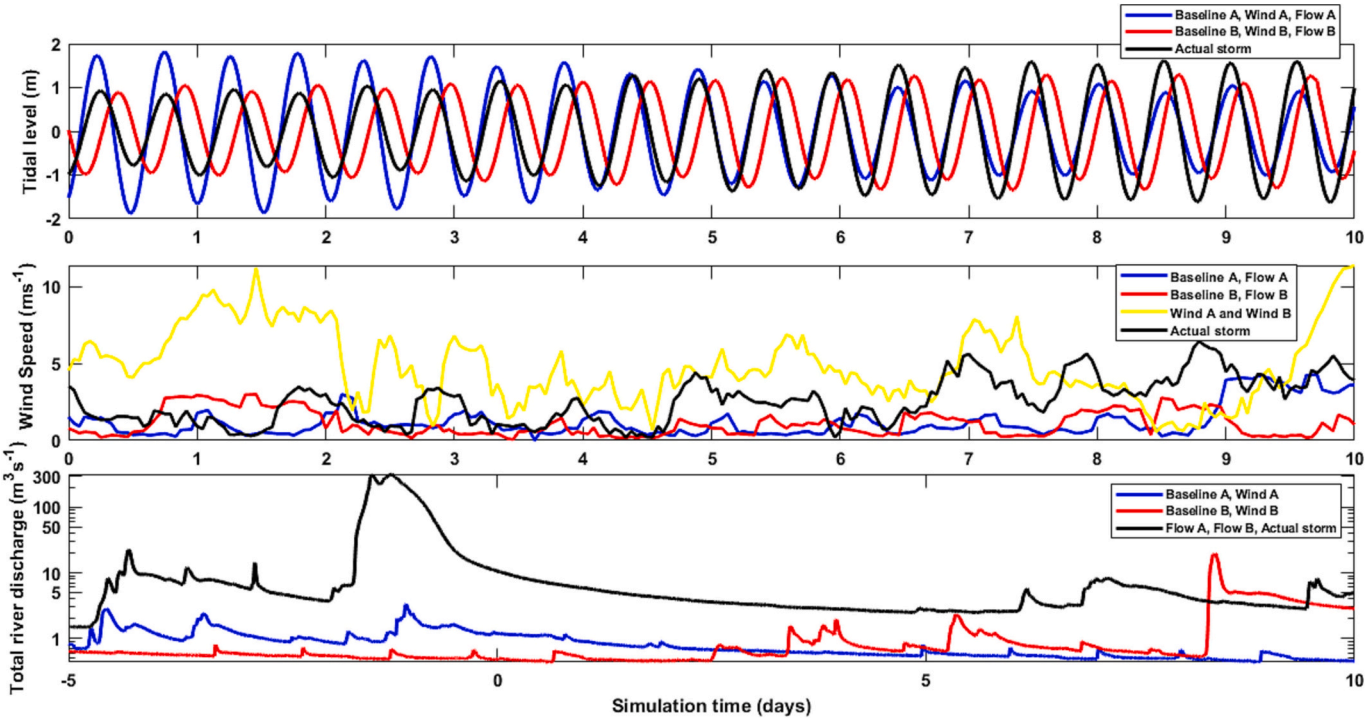

Fig. 3. The tidal level (top), wind speed (middle) and the sum of river discharge (bottom) variation at Stanley Bay in the seven scenarios. The x-axis shows the time relative to the time the floats were launched. Note the y-axis in the river discharge plot is a log scale and the x-axis is extended to five days before float launching, showing the change of freshwater discharge in previous days.

entering the lower channel and the proportion reaching the estuarine mouth. Evaluating the time and proportion of floats entering the lower estuary highlights the mobility of the floats within the estuary between cases. Kauri Point (174.70°E) is chosen as the start of the lower channel as multiple branching creeks converge landward of the point and the main channel bend of almost 90° is a distinctive feature separating the lower and upper estuary. For practical purposes, a float passing beyond the longitude 174.70°E (Fig. 1b) is defined as entering the lower estuary. The proportion of floats that leaves the estuarine mouth (174.81°E) is another key statistic to estimate the likelihood of estuarine plastics entering the open ocean. The mean time floats take to leave the estuarine mouth is a key metric in understanding the rate at which river-sourced plastics are delivered to the ocean. The re-entry rate is calculated to indicate the proportion of floats moving back and forth between

Table 1
Description of the tide, wind and freshwater conditions used in the seven scenarios.

Case	Description
Spring-tide start Baseline (Baseline A)	Floats are launched on Apr 28, 2021, weather and freshwater discharge conditions are from gauged data, validated with spring-tide drifter experiment. Simulation runs for ten days until May 8.
Neap-tide start Baseline (Baseline B)	Floats are launched on May 6, 2021, weather and freshwater discharge conditions are from gauged data, validated with neap-tide drifter experiment. Simulation runs for ten days until May 16.
Strong wind (Wind A and B)	The wind speed and direction are replaced by gauged data on June 15–July 4, 2020, when a storm hit Auckland on June 24. Other conditions held the same as in baseline (one spring-tide start and one neap-tide start run).
High flow (Flow A and B)	The freshwater discharge is replaced by gauged data covering Aug 21-Sep 9, 2021, when a storm hit Auckland. Other conditions are held the same as in baseline cases.
Actual storm	An actual winter storm in August 2021, is simulated. Floats are released on Sep 1. All baseline conditions are replaced by gauged data. The simulation runs for ten days to Sep 11. Freshwater discharge during Actual storm case is the same as Flow A and B.

Table 2
The validation between two baseline simulation cases and drifter observations.

Name	Observations (Spring tide)	Model (Baseline A)	Observations (Neap tide)	Model (Baseline B)
Numbers of drifters	20	250	15	250
Grounded in first tidal cycle	45 %	46 %	80 %	23 %
Grounded in second tidal cycle	50 %	57 %	87 %	88 %
Drifted beyond Harbour Bridge	15 %	5 %	0 %	0 %
Drifted beyond Kauri Point	30 %	20 %	0 %	0 %
Dispersion coefficient along channel	53 m^2/s between ebb peaks; 123 m^2/s in last ebb	90 m^2/s between ebb peaks;161 m^2/s in last ebb	48 m^2/s between ebb peaks; 111 m^2/s in last ebb	39 m^2/s between ebb peaks; 91 m^2/s in last ebb

the lower estuary and the harbour immediately adjacent.

Grounding behaviours are diverse in an estuary. Floats can be grounded permanently, temporarily stranded on a tidal flat and remobilized by the next high tide or wander back and forth with occasional stops (Pawlowicz et al., 2019; Pawlowicz, 2021). These diverse behaviours require a systematic definition to identify the grounding and remobilization. In this model, grounding is defined when a float sits along the shoreline with less than one-metre movement within a five-minute period for more than four consecutive hours. The proportion of grounded floats illustrates how plastic retention is controlled by the hydrodynamics along with the maximum grounding rate and final grounding rate when the simulation finishes. The grounding locations show the retention hotspots of river-sourced plastics between different cases. The magnitude and direction of surface residual circulation near accumulation hotspots are also investigated and contrasted between cases to understand the link between surface flows and floats grounding.

The dispersal of estuarine particles or pollutants due to tides or other hydrodynamics can be described mathematically as the diffusion of a concentration (Fischer et al., 1979). The estimate of along-channel dispersion is calculated from the variance of the along-channel displacement of the ensemble of non-grounded floats. A linear fit to the variance is done using only those floats still floating after seven days. Longitudinal surface dispersion coefficient is estimated using one-half of the gradient of this variance with the launching time ($K_x = 0.5\frac{d\sigma^2}{dt}$;LaCasce, 2008; Chen et al., 2022). Larger dispersion coefficients suggest faster separation within the estuary and quantify the sensitivity to the change of surface flows and grounding.

2.6. Validation of the baseline cases with drifter observations

The validation was carried out by comparing the retention and trajectories of the modelled floats within the first two tidal cycles of the baseline cases (Table 1, Baseline A and B) with the observed drifters (spring-tide and neap-tide drifters; Table 2; Chen et al., 2022). Retention and dispersion patterns of the floats from the baseline simulations are comparable to drifter observations collected over two tidal cycles. In Baseline A, 46 % of the 250 floats ground after the first tidal cycle and 57 % ground after two tidal cycles, which is very close to the observed grounding percentage during spring tides (45 % and 50 %, respectively) (Table 2). Considerably fewer floats in the model drift beyond the Harbour Bridge and Kauri Point compared to the observations. During the last tidal cycle, a higher dispersion coefficient is estimated from the simulation than in the observations. In contrast, during the neap tides, the model underestimates the grounding rate during the first tidal cycle, but the grounding rate from the model reaches a similar level after the second tidal cycle. No floats go beyond Kauri Point in the simulation, which is identical to the observations. The estimate of dispersion coefficients is closer to the observations compared to the spring tide results. In general, the float trajectories in the model are very similar to the observed trajectories from the drifter studies in both the extent they travel within the estuary and the places they go (see Supplementary Fig. S2.7–2.8), which suggests the model provides a good estimate to track buoyant plastic debris.

3. Results

Generally, floats in all the simulations are very likely to be retained in the estuary. The high grounding rates (maximum grounding rates all higher than 90 %; final grounding rates higher than 60 %) and low escape rates (<20 % floats leave the estuarine mouth; Table 3) indicate that most floats launched from the upper channel and branching streams are unlikely to escape the estuarine mouth within ten days. The re-entry rate shows those floats exiting the estuary still have a considerable chance of returning (higher than 60 %). Floats returning to the estuary are likely to ground inside the estuary on their return. As shown in Table 3, the number of floats remaining outside the estuary at the end of the ten-day simulation is at least 25 % smaller than the number of floats that left the estuary.

3.1. Sensitivity of float retention to tides, freshwater discharge and winds

The proportion of floats exiting the estuarine mouth or grounding is modulated by the phase of spring-neap tides. The fast, spring tidal flow in Baseline A brings 2 % of the floats to the estuarine mouth during the second tidal cycle. In contrast, Baseline B begins with weaker neap tides and no floats escape the estuary during the initial few tidal cycles (Fig. 4). The proportion of floats exiting the estuarine mouth in Baseline B rises to 10 % after six days due to the transition from neap to spring tides. In both cases, more floats reach the estuarine mouth when the tides are greater during spring tides. There is little difference of the overall number of floats exiting the estuary at the end of simulations. At the end of the simulation, more Baseline A floats have exited the estuarine mouth than in Baseline B (15 % > 10 %). More Baseline B floats

Table 3
Summary statistics of the simulated floats for the seven scenarios.

Statistics (10 days after launching floats)	Baseline A	Baseline B	Wind A	Wind B	Flow A	Flow B	Actual storm
Floats passing beyond Kauri Point (%)	45	20	54	39	97	56	75
First arrival to Kauri Point (hr)	3	68	13	19	3	31	12
Average time to Kauri Point (hr)	18	138	29	65	23	66	83
Floats passing beyond the estuarine mouth (%)	15	10	17	6	17	8	10
First arrival at the estuarine mouth (hr)	18	130	26	82	23	80	40
Average time to the estuarine mouth (hr)	75	164	91	102	52	105	94
Re-entry rate (%)	87	100	84	100	86	60	96
Floats outside the mouth at the simulation end (%)	5	8	6	1	3	4	6
Maximum grounding rate (%)	94	98	97	99	96	98	97
Final grounding rate (%)	94	62	97	84	96	90	97
Longitudinal dispersion coefficient (m^2/s)	78	16	10	14	77	51	127

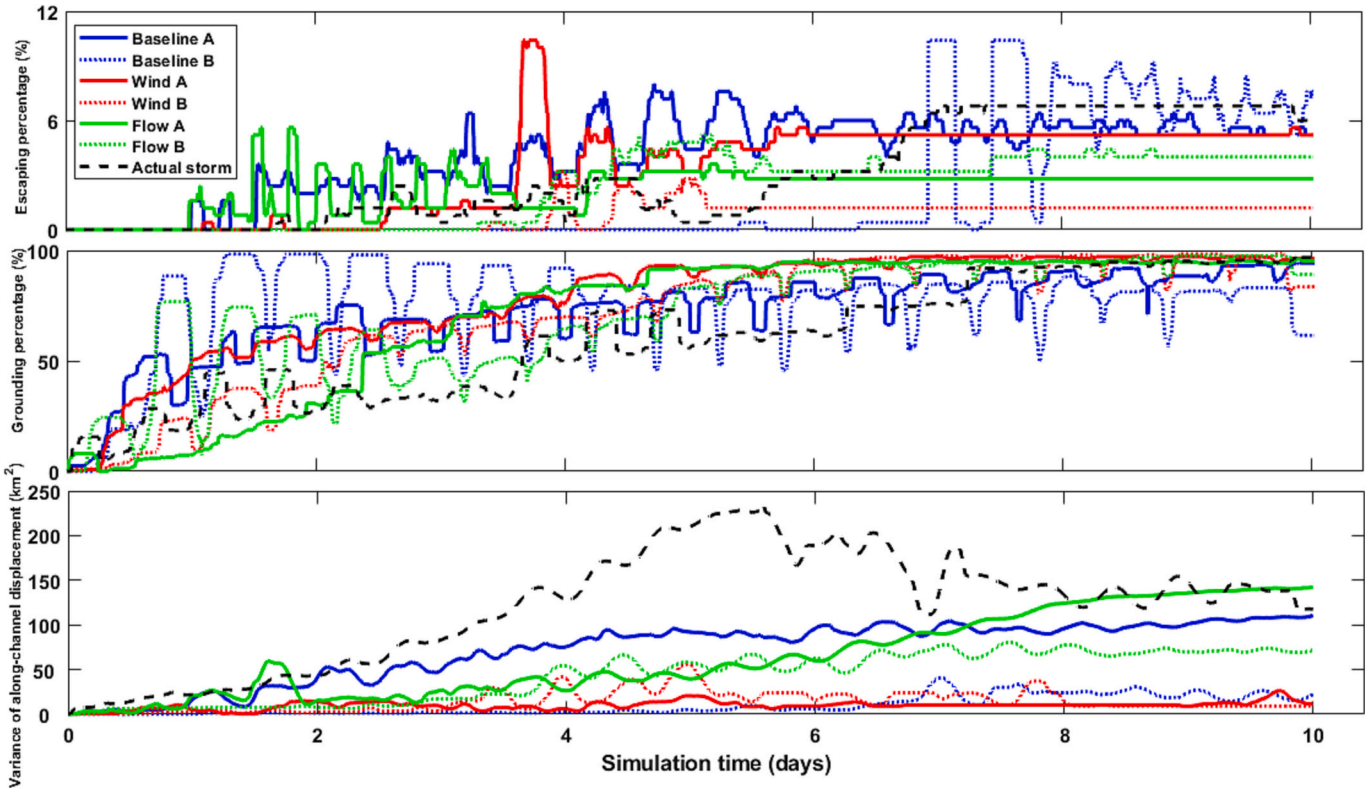

Fig. 4. The percentage of floats escaping the estuarine mouth (top), the grounding percentage of floats (middle) and the ensemble-mean variance of along-channel displacement for non-grounded floats after seven days (bottom) with simulation time for the seven modelling scenarios.

remain outside the estuarine mouth (5 % < 8 %). Additionally, a higher final grounding proportion occurs in Baseline A (94 % > 62 %) while a higher initial grounding proportion occurs in Baseline B (57 % < 88 %). This difference corresponds to the changes in the tidal cycle from spring to neap in Baseline A and neap to spring in Baseline B. More floats are grounded during neap tides and more floats remain floating during spring tides.

The freshwater discharge and wind play smaller roles in moving floats out of the estuary compared to the tides. Simulations with higher river flow (300 m^3s^{-1}) double the proportion of floats entering the lower estuary (up to 97 %) compared to baseline cases (20–45 %), but the number of floats leaving the estuarine mouth remains similar to the baseline cases (<20 %; Table 3). The proportion of floats staying outside the estuary after ten-day simulations (3–4 %) is almost halved in both cases compared to the baseline. The maximum grounding proportion (96 %) and dispersion coefficient (77 m^2s^{-1}) in the Flow A case remain similar to the Baseline A. The final grounding rate (90 %) and dispersion coefficient (51 m^2s^{-1}) are higher in the Flow B case compared to its baseline (Table 3). Higher wind speed slightly increases the maximum grounding probability from 94 % to 99 % and reduces the dispersion down to 10 m^2s^{-1} (Table 3). Compared with the baseline simulations, more floats are transported to the lower estuary with higher wind speed. Only in the Wind A simulation, do more floats pass beyond the estuarine mouth (17 %), with the assistance of the strong wind, while the Wind B case shows the opposite (6 %).

The simulation of the real storm event increases the transport of floats to the lower estuary and limits further transport beyond the estuarine mouth. The Actual storm simulation is configured with high wind, high freshwater flow and neap tides, and therefore, the float behaviour contains features from both Wind B and Flow B cases. The combination of high wind speed and freshwater flow hastens the downstream transport of floats to the lower estuary resulting in the highest number passing beyond Kauri Point (75 %) among all neap-start simulations. The percentage of floats that have left the estuarine mouth (10 %; Table 3) is smaller than the Baseline B. The maximum grounding rate (97 %) is similar to the Wind B and Flow B cases. The initial dispersion during the Actual storm simulation is markedly larger than the other neap-start cases and reaches the highest level of all simulations

(127 m^2s^{-1}; Fig. 4).

3.2. Float grounding locations and the surface residual currents

Floats are grounded near their launching locations unless faster surface flows (during spring tides or after high discharge) aid in transporting them to the lower estuary (Fig. 5). The grounding location is modulated by the change of tides. More Baseline A floats are retained along the north shore of the lower estuary, while the west banks of the upper estuary trap more floats in the Baseline B case (Fig. 5a). The strong easterlies in both Wind A and Wind B cause floats to ground along the west bank of the upper estuary (Fig. 5b). In the other three cases with high freshwater discharge (Flow A, Flow B and Actual storm), the grounding locations shift to the bays of the northern shore in the lower estuary (Fig. 5c-d). This shows increased downstream surface flow transports more floats to the lower estuary, but those floats tend to ground there rather than leave the estuary.

We explore the connection between grounding locations and the surface residual currents averaged over the first four days in each scenario (Fig. 6). There is little difference in the surface residual currents between spring and neap tides (Fig. 6a-c). The wind cases (Fig. 6d-e) illustrate very similar patterns of surface residual currents inside the estuary compared to the baseline cases. However, near the mouth, strong easterlies create surface residual currents towards land (Fig. 6j). Floats near the estuarine mouth drift back onshore and ground, leading to a marked reduction in the number of floats remaining outside the estuary during the Wind B case (1 %) compared to Baseline B (8 %). Increased river flow leads to faster subtidal currents in the central upper channel compared to baseline cases (Fig. 6f-g), which results in more floats entering the lower estuary. Residual flows are stronger by 0.05 ms^{-1} towards the northern shore in the lower estuary (Fig. 6k). This lateral circulation leads to grounding in the lower estuary and prevents the floats from leaving the estuary. Similar patterns can be found in the Actual storm simulation (Fig. 6h and l) from the combination of strong wind and high freshwater discharge (Fig. 6e and g).

3.3. Salinity gradient drives lateral circulation

We investigate whether the high grounding rate and low escape rate in the lower estuary during high flow and storm cases is due to the response of the lateral circulation created by changes in the lateral salinity gradient as noted in other estuaries (Valle-Levinson, 2010; Lerczak and Geyer, 2004). We select a float retention hotspot on the northern shore 3 km downstream of Kauri Point and project the velocities along a line perpendicular to the main channel (Fig. 7a). The depth-averaged velocity is subtracted to remove changes due to average tidal and riverine flows. The velocity (u) and lateral salinity gradient ($\partial S/\partial y$) in the Flow A simulation are plotted three days after the peak freshwater discharge at four different phases of the tide as well as the tidal average (Fig. 7b-k).

Smaller escape rate occurs when there is stronger lateral circulation and a stronger lateral salinity gradient in the high flow scenarios. In Baseline A, the surface lateral circulation along the cross-section is weak, with residual surface flows <0.02 ms^{-1}, but follows a classical density-driven pattern (Nunes and Simpson, 1985). In this classical pattern, flows diverge from the centre of the estuary, when lower salinity values occur at the surface during late ebb tides and converge towards the centre of the channel during late flood tides when salinities there are higher. In the simulations with high discharge (Flow A; Fig. 7g-j), the lateral salinity gradient is intensified compared to Baseline A (Fig. 8g-j), which enhances the lateral flows at the surface (Fig. 8b-e). The lateral salinity gradient at ebb maximum (Fig. 7g) is the strongest, especially near the southern bank, resulting in strengthened northbound surface flow over the whole transect (Fig. 7b). The lateral salinity reduces on the northern shore during the low slack tide (Fig. 7h), developing divergent surface flows (Fig. 7c). The northbound surface flow and the divergent currents during ebb tides would move the floats northward, contributing to the increased grounding between Kauri Point and the estuarine mouth. The reversed lateral salinity gradient (Fig. 7i-j) and convergent surface flow (Fig. 7d-e) develop during the flood tide and continue at high slack tide, which may pick up some grounded floats. During these phases of the tide, the non-grounded particles are aggregated in the channel centre and moved landward, increasing retention in the estuary. The lateral velocity is weaker during flood tides

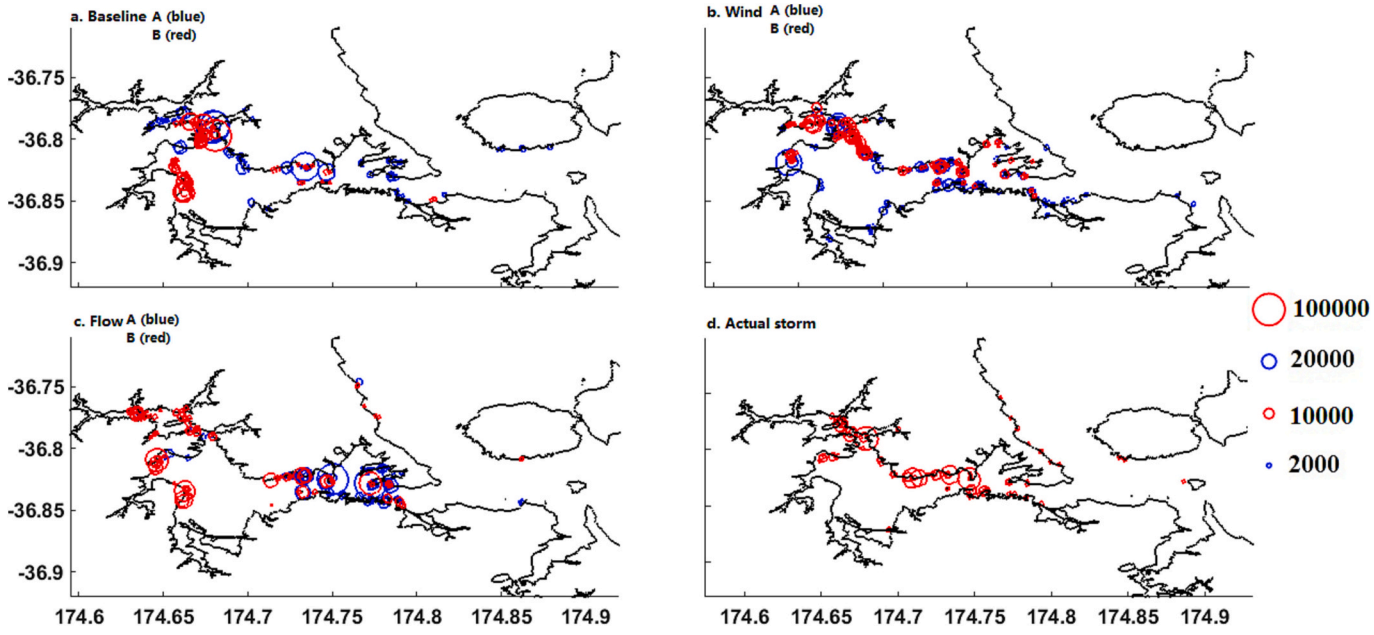

Fig. 5. Circles illustrate where the floats accumulated in the seven simulations: a. Baseline A (blue) and Baseline B (red); b. Wind A (blue) and Wind B (red); c. Flow A (blue) and Flow B (red); d. Actual storm. The size of the circle refers to the sum of floats grounded there in each five-minute interval over the whole simulation, as noted on the legend. (For interpretation of the references to colour in this figure legend, the reader is referred to the web version of this article.)

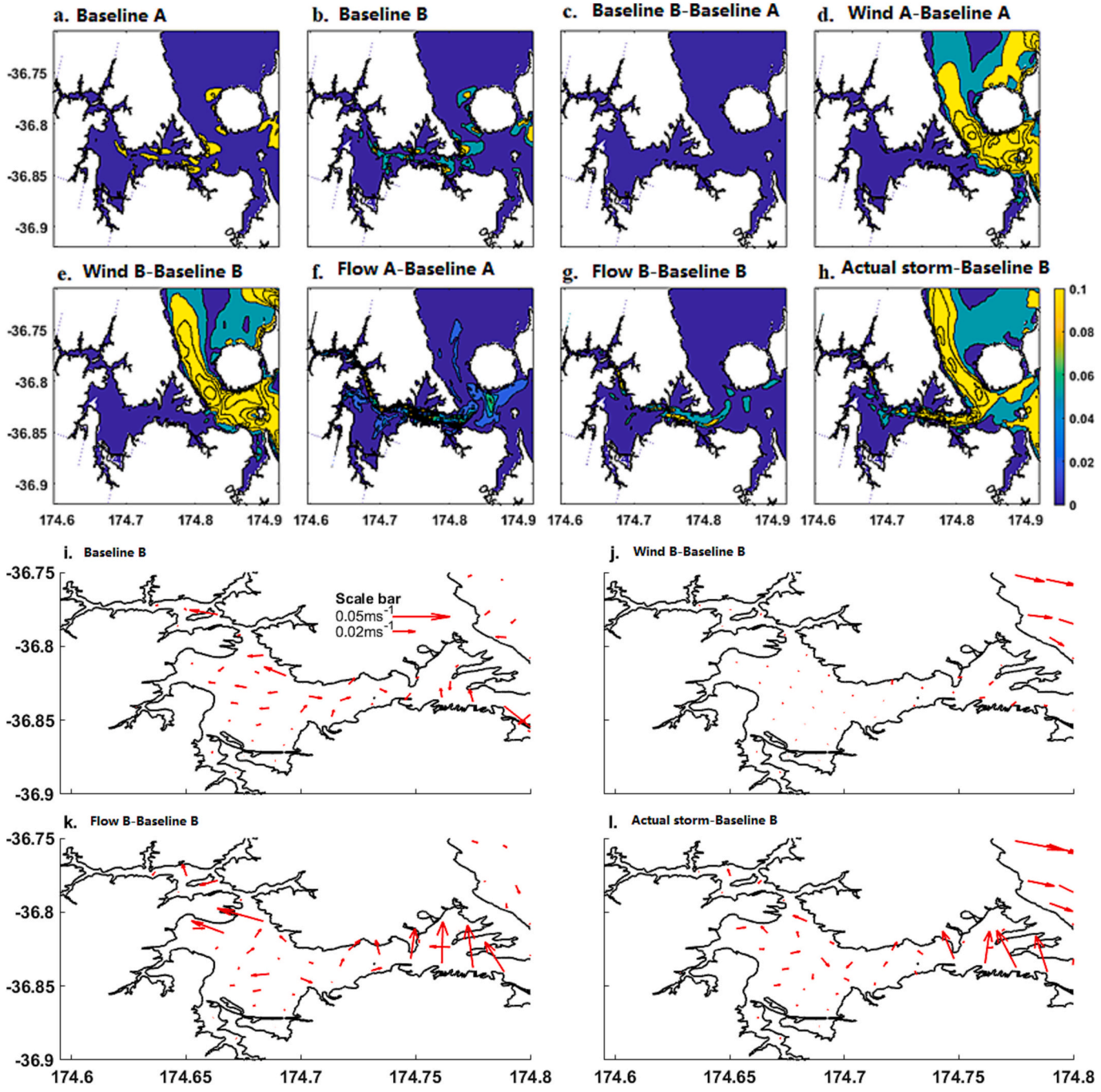

Fig. 6. Top: the magnitude of surface residual currents averaged over the first four days after float launching during different scenarios. a. Baseline A; b. Baseline B; c. the difference between Baseline B and Baseline A; d. the difference between Wind A and Baseline A; e. the difference between Wind B and Baseline B; f. the difference between Flow A and Baseline A; g. the difference between Flow B and Baseline B; h. the difference between Actual storm and Baseline B; Bottom: the magnitude and direction of surface residual currents shown by arrows in selected locations: i. Baseline B; j. the difference between Wind B and Baseline B; k. the difference between Flow B and Baseline B; l. the difference between Actual storm and Baseline B.

compared to ebb tides, leading to a subtidal northbound surface velocity (increasing to 0.05 ms^{-1}) over almost the entire transect (Fig. 7f). Therefore, this enhanced lateral circulation after high discharge produces more retention during flood tides and stronger flow towards the banks during ebb tides. The increased subtidal northbound flow also increases the chance of grounding along the northern shore of the lower estuary.

4. Discussion

The tide is the dominant factor determining the escape of plastic from the estuary. More floats are transported out of the estuary during spring tides than neap tides (for example, 10 % vs. 0 % in Baseline B; Fig. 4). Floats are more likely to ground during neap tides (over 80 %; Fig. 4). The water level is much higher during spring high slack tides than the neap, which submerges more area at the edge. During the following ebb tides, the floats in the upper estuary can be transported further downstream with less chance to be grounded at the channel edge

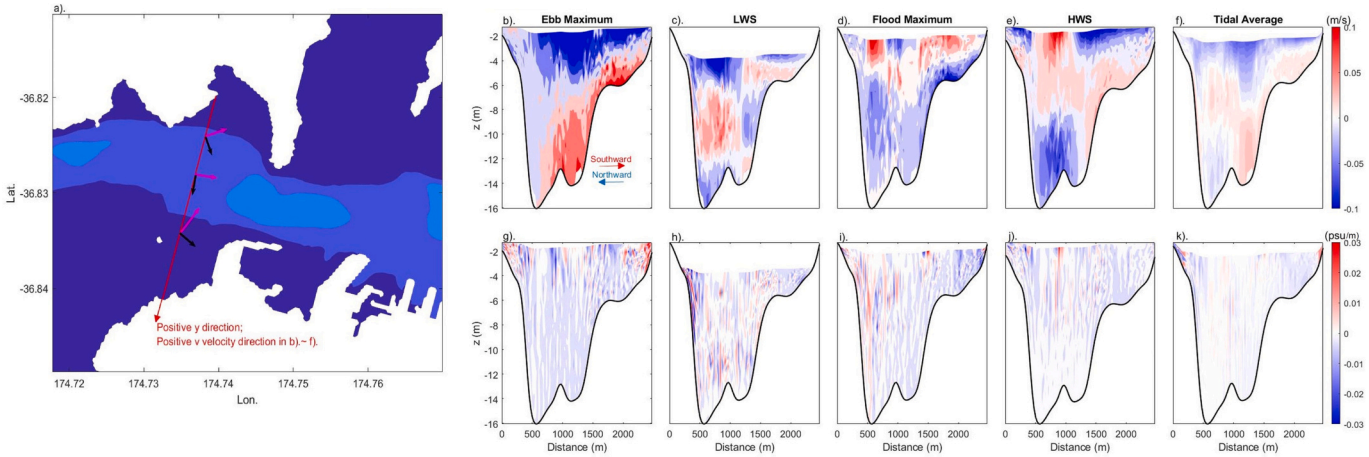

Fig. 7. The velocity and salinity gradient along the cross-section three days after peak freshwater discharge in case Flow A. Red line in a) marks the transect where magenta arrows indicate the principal tidal current directions along the transect, black arrows indicate the direction orthogonal to it. The panels b) - e) refers to the lateral velocity at ebb maximum, low water slack (LWS), flood maximum and high water slack (HWS), respectively. Panels g) ~ j) follow the same order showing the variation of lateral salinity gradient. Panel f) shows the subtidal lateral velocity (averaged over a tidal cycle) and Panel k) shows the subtidal lateral salinity gradient. $y = 0$ corresponds to the north end of the transect. Negative (blue) values represent currents flowing (along the transect) towards the northern bank (shown by arrows) and reduced salinity from the south to the north bank. (For interpretation of the references to colour in this figure legend, the reader is referred to the web version of this article.)

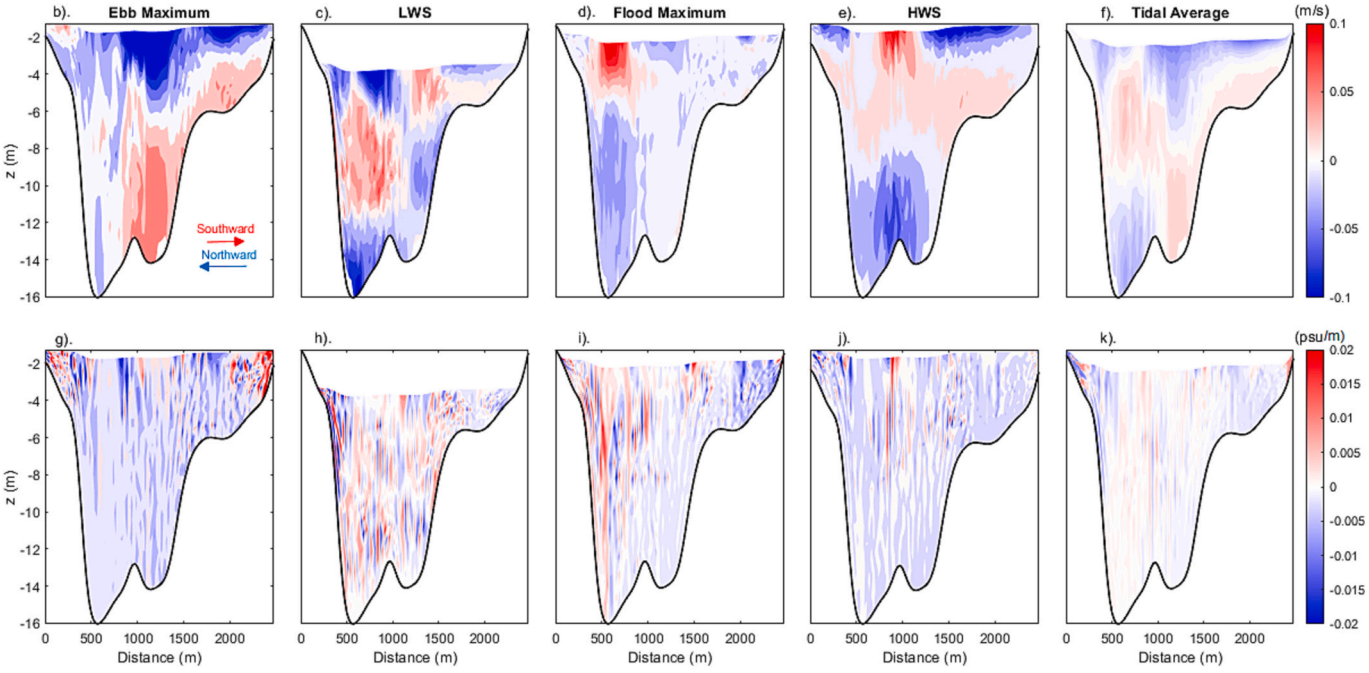

Fig. 8. The difference of velocity and salinity gradient along the cross-section three days after peak freshwater discharge between Flow A and Baseline A. The subplots b-k follow the same order and format as Fig. 7b-k.

(Chen et al., 2022). The surface tidal current is faster during spring tides, which also enhances the downstream travelling distance of floats during ebb tides and helps more floats exiting the estuary.

The high freshwater discharge after the storm does not move more floats out of the estuarine mouth but leads to similar grounding percentages (over 90 %) inside the estuary. These results suggest that <20 % of river-sourced buoyant plastics exit the estuary regardless of the freshwater flow. Plastics that have left the estuarine mouth are likely (60 %) to re-enter the estuary and may be retained for long times. The low escape rates after high freshwater discharge challenge the observations in other estuaries that high river flows are the best times for buoyant plastics to escape (van Emmerik et al., 2019b; Krelling and Turra, 2019). The high downstream transport from the upper to lower estuary (up to 97 %) and low escape rate of floats from the estuary (<20 %) highlight the dual effects of freshwater discharge on buoyant particle transport in an estuary. Freshwater flow increases the downstream transport along the channel and also enhances grounding by creating a stronger density-driven lateral circulation (Figs. 7-8). The impact of freshwater discharge on plastic retention needs further investigation in future. For example, increasing stratification may initially increase the lateral circulation, but may reach a threshold where it shuts down the lateral circulation due to the isopycnal-tilting by the vertical velocity (Lerczak and Geyer, 2004). More observations in well-mixed estuaries are needed to establish if and when this threshold is reached.

The simulation outcomes suggest that river-sourced buoyant plastics have a very high chance to ground and be retained in estuaries such as the Waitematā. During high river discharge, the downstream plastic transport in the upper estuary is largely enhanced, which is consistent with studies in estuaries with a long channel, such as the Seine River (van Emmerik et al., 2019b) and Rhine River (van Emmerik et al., 2022b). However, the Waitematā is shorter than these estuaries, yet our results show a marked plastic retention due to onshore residual flows in the lower estuary. Retention in the Waitematā is likely similar to Willapa Bay, located on the Washington coast of the USA, which has similarly branched channels, a high tidal exchange rate, and low river discharge during the summer. Banas and Hickey (2005) find that passive particles are retained for 3–5 weeks in the upper estuary of Willapa Bay. These retention rates would likely lead to high concentration of plastics on the shorelines, mixing with sediment, and degradation into microplastics in this type of estuary (Lahens et al., 2018; Schreyers et al., 2023). The outcomes of this study can also be applied to similar type of estuaries in New Zealand or globally, for example, Whangarei Harbour and Otago Harbour (Williams, 1986), Yaquina Bay (Lemagie and Lerczak, 2015).

Our results show locally produced litter is likely largely retained locally in this type of estuary even after storms. These results support recommendations of regular clean-ups along the shoreline (Andrady, 2017; Yao et al., 2019) to prevent plastics from entering the ocean. Higher grounding proportion during neap tides indicates that neap tide is the better time to organise the clean-ups than spring tides. In addition, global models of plastic emission need to consider the estuarine retention in order to properly account for the current overestimate of riverine plastic entering the ocean. Although progresses on modelling relationships between river discharge, tidal dynamics and plastic export rate have been made in this study and several other studies (Gisen and Savenije, 2015; van Emmerik et al., 2022b; Schreyers et al., 2023), more observational or numerical studies of plastic transport and retention are needed to account for these types of estuaries globally.

Several improvements could be made in future studies of plastic motion in an estuary. Floats in this study represent the transport of most buoyant plastics with little windage. For instance, the outcomes of this study can be applied to predicting the transport of filled plastic shopping bags, food containers, submerged bottles and all buoyant plastic fragments. Larger plastics whose trajectories include motion due to windage and wind-driven waves are expected to have higher chance of grounding as swash waves and winds push them to the upper backshore along the shorelines (Hinata et al., 2017). Wind-driven waves will be considered in future numerical studies to simulate the transport of large plastics. The transport and retention behaviours are also dependent on the geometry and size of plastic items (Schreyers et al., 2023; Pawlowicz, 2021; Ryan, 2021), which are not considered in our simulations. In addition, transport of particles with sinking behaviour due to sources of higher density plastics or from flocculation and biofouling of buoyant plastics with time (Laursen et al., 2023; Schwarz et al., 2019) are expected to be considerably different from buoyant particles (Francalanci et al., 2021). Future numerical studies in the Waitematā Estuary aim to simulate the fate of sinking plastic particles as well.

More detailed studies are needed to unravel the role of river discharge in the transport and retention of buoyant particles through an estuarine environment. The launching locations have been selected to represent the two largest freshwater sources, however the occurrence of plastics is complex and related to human activities: more plastic waste is dumped on shorelines and streams near the industrial and residential areas (Gregory, 1978). Therefore, smaller creeks may contain more plastics if they are close to densely populated areas (for example, Whau River). The simulations also indicate that high discharge redistributes the retention of buoyant plastics within the estuary by remobilizing more plastics and bringing them to the lower estuary. Future field observations of the transport of plastics during high river discharge (for example, van Emmerik et al., 2019b) are needed to clarify the role of river discharge in transporting buoyant particles and verify the model results.

5. Conclusion

The ten-day float simulations show the sensitivity of mobility and grounding of river-sourced buoyant plastics in a well-mixed estuary to different tides, winds, and freshwater discharge. All simulations have high rates of float grounding (over 60 %) and <20 % of the floats leave the estuary after ten days. Spring tides allow more floats escape the estuary than neap tides. Greater freshwater discharge leads to a marked increase (up to 97 %) in floats transported to the lower estuary. However, over 90 % of the floats still ground when river discharge is high, similar to cases with low river discharge, and the number of floats leaving the estuarine mouth is not markedly increased. We show that the enhanced grounding in the lower estuary is due to a doubling of the strength of the density-driven lateral flows that move the floats towards the banks. The high grounding rates and low escape rates suggest that global models may overestimate the amount of plastic entering the ocean from estuaries and some estuaries may trap most of buoyant plastic litter regardless of the winds, tides or freshwater flow. These results emphasise the role of local clean-ups as an extremely effective means of preventing future plastic pollution in the ocean.

CRediT authorship contribution statement

Zheng Chen: Conceptualization, Hydrodynamic modelling, Float modelling scenario designs, Writing offline modelling codes, Float validation, Formal analysis, General investigation, Data Curation, Writing - Original Draft, Response to reviewers' comments.

Gaoyang Li: Conceptualization, Hydrodynamic modelling, Writing - Hydrodynamic modelling method, Velocity and salinity validation, Investigating lateral flow at the lower estuary.

Melissa Bowen: Conceptualization, Methodology, Validation, Writing - Review & Editing, Supervision, Response to reviewers' comments.

Giovanni Coco: Conceptualization, Methodology, Validation, Proof reading, Supervision.

Declaration of competing interest

The authors declare that they have no known competing financial interests or personal relationships that could have appeared to influence the work reported in this paper.

Data availability

The data and codes used in this paper is published on the University of Auckland data repository website Figshare. (Link attached in the manuscript acknowledgement).

Acknowledgement

We would like to thank New Zealand eScience Institution (NeSI) for providing the two high performance computers Maui and Mahuika to run the model. We appreciate the bathymetry data sharing from the Auckland Council, LINZ and NIWA. Z.C. and G.L. are supported by University of Auckland Doctoral Scholarship. The study was funded by Aotearoa Impacts & Mitigation of Microplastics by the NZ Ministry of Business, Innovation and Employment and supported M.B. and G.C. The field equipment in model validation was provided by the University of Auckland and installed by technicians Brendan Hall and David Wackrow from the School of Environment and also the team on board the research vessel Hawere from the Institute of Marine Science and School of Biological Science. We also appreciate the help from local communities: River Care Group, Ecomatters, Seacleaners, Hobsonville ferry service by Auckland Transport, Devonport naval base. Data, codes and videos are

published on figshare.com: https://doi.org/10.17608/k6.auckland.23255180. Other data are available on request to the author.

Appendix A. Supplementary data

Supplementary data to this article can be found online at https://doi.org/10.1016/j.marpolbul.2023.115395.

References

Andrady, A.L., 2011. Microplastics in the marine environment. Mar. Pollut. Bull. 62 (8), 1596–1605.

Andrady, A.L., 2017. The plastic in microplastics: a review. Mar. Pollut. Bull. 119 (1), 12–22.

Atwood, E.C., Falcieri, F.M., Piehl, S., Bochow, M., Matthies, M., Franke, J., Siegert, F., 2019. Coastal accumulation of microplastic particles emitted from the Po River, Northern Italy: comparing remote sensing and hydrodynamic modelling with in situ sample collections. Mar. Pollut. Bull. 138, 561–574.

Balas, C.E., Williams, A.T., Simmons, S.L., Ergin, A., 2001. A statistical riverine litter propagation model. Mar. Pollut. Bull. 42 (11), 1169–1176.

Banas, N.S., Hickey, B.M., 2005. Mapping exchange and residence time in a model of Willapa Bay, Washington, a branching, macrotidal estuary. J. Geophys. Res. Oceans 110 (C11).

Bellasi, A., Binda, G., Pozzi, A., Galafassi, S., Volta, P., Bettinetti, R., 2020. Microplastic contamination in freshwater environments: a review, focusing on interactions with sediments and benthic organisms. Environments 7 (4), 30.

Blettler, M.C., Abrial, E., Khan, F.R., Sivri, N., Espinola, L.A., 2018. Freshwater plastic pollution: recognizing research biases and identifying knowledge gaps. Water Res. 143, 416–424.

Blondel, E., Buschman, F.A., 2022. Vertical and horizontal plastic litter distribution in a bend of a tidal river. Front. Environ. Sci. 10, 587.

Bridson, J.H., Patel, M., Lewis, A., Gaw, S., Parker, K., 2020. Microplastic contamination in Auckland (New Zealand) beach sediments. Mar. Pollut. Bull. 151, 110867.

Cardoso-Mohedano, J.G., Ruiz-Fernández, A.C., Sanchez-Cabeza, J.A., Camacho-Torres, S.M., Ontiveros-Cuadras, J.F., 2023. Microplastics transport in a low-inflow estuary at the entrance of the Gulf of California. Sci. Total Environ. 161825.

Chen, Z., Bowen, M.M., 2020. Observations of salinity, flushing time and dispersion in the Waitemata Estuary. N. Z. J. Mar. Freshw. Res. 56 (1), 59–77.

Chen, Z., Bowen, M., Li, G., Coco, G., Hall, B., 2022. Retention and dispersion of buoyant plastic debris in a well-mixed estuary from drifter observations. Mar. Pollut. Bull. 180, 113793.

CliFlo, N.I.W.A., 2021. New Zealand's National Climate Database. National Institute of Water and Atmospheric Research New Zealand (NIWA).

Collins, C., Hermes, J.C., 2019. Modelling the accumulation and transport of floating marine micro-plastics around South Africa. Mar. Pollut. Bull. 139, 46–58.

Dikareva, N., Simon, K.S., 2019. Microplastic pollution in streams spanning an urbanisation gradient. Environ. Pollut. 250, 292–299.

Duncan, E.M., Davies, A., Brooks, A., Chowdhury, G.W., Godley, B.J., Jambeck, J., Koldewey, H., 2020. Message in a bottle: open source technology to track the movement of plastic pollution. PLoS One 15 (12), e0242459.

Egbert, G.D., Erofeeva, S.Y., 2002. Efficient inverse modeling of barotropic ocean tides. J. Atmos. Ocean. Technol. 19 (2), 183–204.

Fischer, H.B., List, J.E., Koh, C.R., Imberger, J., Brooks, N.H., 1979. Mixing in Inland and Coastal Waters. Academic press.

Francalanci, S., Paris, E., Solari, L., 2021. On the prediction of settling velocity for plastic particles of different shapes. Environ. Pollut. 290, 118068.

Gérigny, O., Pedrotti, M.L., El Rakwe, M., Brun, M., Pavec, M., Henry, M., Galgani, F., 2022. Characterization of floating microplastic contamination in the bay of Marseille (French Mediterranean Sea) and its impact on zooplankton and mussels. Mar. Pollut. Bull. 175, 113353.

Gisen, J.I.A., Savenije, H.H., 2015. Estimating bankfull discharge and depth in ungauged estuaries. Water Resour. Res. 51 (4), 2298–2316.

Green, M.O., Hancock, N.J., 2012. Sediment transport through a tidal creek. Estuar. Coast. Shelf Sci. 109, 116–132.

Gregory, M.R., 1978. Accumulation and distribution of virgin plastic granules on New Zealand beaches. N. Z. J. Mar. Freshw. Res. 12 (4), 399–414.

Haidvogel, D.B., Arango, H., Budgell, W.P., Cornuelle, B.D., Curchitser, E., Di Lorenzo, E., Wilkin, J., 2008. Ocean forecasting in terrain-following coordinates: formulation and skill assessment of the Regional Ocean modeling system. J. Comput. Phys. 227 (7), 3595–3624.

Hersbach, H., Bell, B., Berrisford, P., Hirahara, S., Horányi, A., Muñoz-Sabater, J., Thépaut, J.N., 2020. The ERA5 global reanalysis. Q. J. R. Meteorol. Soc. 146 (730), 1999–2049.

Hinata, H., Mori, K., Ohno, K., Miyao, Y., Kataoka, T., 2017. An estimation of the average residence times and onshore-offshore diffusivities of beached microplastics based on the population decay of tagged meso-and macrolitter. Mar. Pollut. Bull. 122 (1–2), 17–26.

Hong, S., Lee, J., Lim, S., 2017. Navigational threats by derelict fishing gear to navy ships in the Korean seas. Mar. Pollut. Bull. 119 (2), 100–105.

Honingh, D., Van Emmerik, T., Uijttewaal, W., Kardhana, H., Hoes, O., Van de Giesen, N., 2020. Urban river water level increase through plastic waste accumulation at a rack structure. Front. Earth Sci. 8, 28.

Hope, J.A., Coco, G., Ladewig, S.M., Thrush, S.F., 2021. The distribution and ecological effects of microplastics in an estuarine ecosystem. Environ. Pollut. 288, 117731.

Huhn, F., von Kameke, A., Allen-Perkins, S., Montero, P., Venancio, A., Perez-Munuzuri, V., 2012. Horizontal Lagrangian transport in a tidal-driven estuary—transport barriers attached to prominent coastal boundaries. Cont. Shelf Res. 39, 1–13.

Hume, T., 2018. Fit of the ETI trophic state susceptibility typology to the NZ coastal hydrosystems classification. In: NIWA Client Report, 34.

Hume, T.M., Snelder, T., Weatherhead, M., Liefting, R., 2007. A controlling factor approach to estuary classification. Ocean Coast. Manag. 50, 905–929.

ICNZ, 2021. Cost of natural disasters. Retrieved December 03 from. https://www.icnz.org.nz/natural-disasters/cost-of-natural-disasters.

Krelling, A.P., Turra, A., 2019. Influence of oceanographic and meteorological events on the quantity and quality of marine debris along an estuarine gradient. Mar. Pollut. Bull. 139, 282–298.

LaCasce, J., 2008. Statistics from Lagrangian observations. Prog. Oceanogr. 77 (1), 1–29.

Lahens, L., Strady, E., Kieu-Le, T.C., Dris, R., Boukerma, K., Rinnert, E., Tassin, B., 2018. Macroplastic and microplastic contamination assessment of a tropical river (Saigon River, Vietnam) transversed by a developing megacity. Environ. Pollut. 236, 661–671.

Laursen, S.N., Fruergaard, M., Dodhia, M.S., Posth, N.R., Rasmussen, M.B., Larsen, M.N., Andersen, T.J., 2023. Settling of buoyant microplastic in estuaries: the importance of flocculation. Sci. Total Environ. 886, 163976.

Lebreton, L., Van Der Zwet, J., Damsteeg, J.W., Slat, B., Andrady, A., Reisser, J., 2017. River plastic emissions to the world's oceans. Nat. Commun. 8 (1), 1–10.

Lemagie, E.P., Lerczak, J.A., 2015. A comparison of bulk estuarine turnover timescales to particle tracking timescales using a model of the Yaquina Bay estuary. Estuar. Coasts 38, 1797–1814.

Lerczak, J.A., Geyer, W.R., 2004. Modeling the lateral circulation in straight, stratified estuaries. J. Phys. Oceanogr. 34 (6), 1410–1428.

Li, M., Zhong, L., Boicourt, W.C., 2005. Simulations of Chesapeake Bay estuary: sensitivity to turbulence mixing parameterizations and comparison with observations. J. Geophys. Res. Oceans 110 (C12).

Lima, A.R., Silva, M.D., Possatto, F.E., Ferreira, G.V., Krelling, A.P., 2020. Plastic contamination in Brazilian freshwater and coastal environments: a source-to-sea transboundary approach. In: Plastics in the Aquatic Environment-Part I. Springer, Cham, pp. 427–460.

Mackay, K.A., Mackay, E.J., Neil, H.L., Mitchell, J.S., Bardsley, S.A., 2012. Hauraki Gulf. NIWA Chart, Miscellaneous Series, p. 91.

Mai, L., Sun, X.F., Xia, L.L., Bao, L.J., Liu, L.Y., Zeng, E.Y., 2020. Global riverine plastic outflows. Environ. Sci. Technol. 54 (16), 10049–10056.

Martínez-Vicente, V., Clark, J.R., Corradi, P., Aliani, S., Arias, M., Bochow, M., Vethaak, A.D., 2019. Measuring marine plastic debris from space: initial assessment of observation requirements. Remote Sens. 11 (20), 2443.

Mcllgorm, A., Raubenheimer, K., Mcllgorm, D.E., 2020. Update of 2009 APEC Report on Economic Costs of Marine Debris to APEC Economies. APEC, Australia.

Meijer, L.J., van Emmerik, T., van der Ent, R., Schmidt, C., Lebreton, L., 2021. More than 1000 rivers account for 80% of global riverine plastic emissions into the ocean. Sci. Adv. 7 (18), eaaz5803.

Newbould, R.A., Powell, D.M., Whelan, M.J., 2021. Macroplastic debris transfer in rivers: a travel distance approach. Front.Water 111.

Nunes, R.A., Simpson, J.H., 1985. Axial convergence in a well-mixed estuary. Estuar. Coast. Shelf Sci. 20 (5), 637–649.

Pawlowicz, R., 2021. The grounding of floating objects in a marginal sea. J. Phys. Oceanogr. 51 (2), 537–551.

Pawlowicz, R., Hannah, C., Rosenberger, A., 2019. Lagrangian observations of estuarine residence times, dispersion, and trapping in the Salish Sea. Estuar. Coast. Shelf Sci. 225, 106246.

Pereiro, D., Souto, C., Gago, J., 2018. Calibration of a marine floating litter transport model. J. Oper. Oceanogr. 11 (2), 125–133.

Pinheiro, L.M., Agostini, V.O., Lima, A.R.A., Ward, R.D., Pinho, G.L.L., 2021. The fate of plastic litter within estuarine compartments: an overview of current knowledge for the transboundary issue to guide future assessments. Environ. Pollut. 279, 116908.

Ryan, P., 2021. Does size and buoyancy affect the long-distance transport of floating debris? Environ. Res. Lett. 10, 2021. https://doi.org/10.1016/j.ecss.2021.107186.

Ryan, P.G., Perold, V., 2021. Limited dispersal of riverine litter onto nearby beaches during rainfall events. Estuar. Coast. Shelf Sci. 251, 107186.

Schmidt, C., Krauth, T., Wagner, S., 2017. Export of plastic debris by rivers into the sea. Environ. Sci. Technol. 51 (21), 12246–12253.

Schreyers, L.D.M., van Emmerik, T.H.M., Bui, K., Van Le Thi, K., Vermeulen, B., Nguyen, H.-Q., van der Ploeg, M., 2023. Tidal dynamics limit river plastic transport. EGUsphere 2023. https://doi.org/10.5194/egusphere-2022-1495 (preprint).

Schwarz, A.E., Ligthart, T.N., Boukris, E., Van Harmelen, T., 2019. Sources, transport, and accumulation of different types of plastic litter in aquatic environments: a review study. Mar. Pollut. Bull. 143, 92–100.

Shchepetkin, A.F., McWilliams, J.C., 2005. The regional oceanic modeling system (ROMS): a split-explicit, free-surface, topography-following-coordinate oceanic model. Ocean Model 9 (4), 347–404.

Strand, K.O., Huserbråten, M., Dagestad, K.F., Mauritzen, C., Grøsvik, B.E., Nogueira, L. A., Röhrs, J., 2021. Potential sources of marine plastic from survey beaches in the Arctic and Northeast Atlantic. Sci. Total Environ. 790, 148009.

Thiel, M., Luna-Jorquera, G., Álvarez-Varas, R., Gallardo, C., Hinojosa, I.A., Luna, N., Miranda-Urbina, D., Morales, N., Ory, N., Pacheco, A.S., Portflitt-Toro, M., 2018. Impacts of marine plastic pollution from continental coasts to subtropical gyres—fish, seabirds, and other vertebrates in the SE Pacific. Front. Mar. Sci. 238.

Thompson, R.C., 2015. Microplastics in the marine environment: sources, consequences and solutions. In: Marine Anthropogenic Litter. Springer, Cham, pp. 185–200.
Thyng, K.M., Kobashi, D., Ruiz-Xomchuk, V., Qu, L., Chen, X., Hetland, R.D., 2021. Performance of offline passive tracer advection in the Regional Ocean Modeling System (ROMS; v3. 6, revision 904). Geosci. Model Dev. 14 (1), 391–407.
Tramoy, R., Colasse, L., Gasperi, J., Tassin, B., 2019. Plastic debris dataset on the Seine river banks: plastic pellets, unidentified plastic fragments and plastic sticks are the Top 3 items in a historical accumulation of plastics. Data in brief 23, 103697.
Tramoy, R., Gasperi, J., Colasse, L., Silvestre, M., Dubois, P., Noûs, C., et al., 2020a. Transfer dynamics of macroplastics in estuaries–new insights from the Seine estuary: part 2. Short-term dynamics based on GPS-trackers. Mar. Pollut. Bull. 160, 111566 https://doi.org/10.1016/j.marpolbul.2020.111566.
Tramoy, R., Gasperi, J., Colasse, L., Tassin, B., 2020b. Transfer dynamic of macroplastics in estuaries—new insights from the Seine estuary: part 1. Long term dynamic based on date-prints on stranded debris. Mar. Pollut. Bull. 152, 110894 https://doi.org/10.1016/j.marpolbul.2020.110894.
Valle-Levinson, A. (Ed.), 2010. Contemporary Issues in Estuarine Physics. Cambridge University Press.
van Emmerik, T., Schwarz, A., 2020. Plastic debris in rivers. Wiley Interdiscip. Rev. Water 7 (1), e1398.
van Emmerik, T., Loozen, M., Van Oeveren, K., Buschman, F., Prinsen, G., 2019a. Riverine plastic emission from Jakarta into the ocean. Environ. Res. Lett. 14, 084033 https://doi.org/10.1088/1748-9326/ab30e8.
van Emmerik, T., Tramoy, R., Van Calcar, C., Alligant, S., Treilles, R., Tassin, B., Gasperi, J., 2019b. Seine plastic debris transport tenfolded during increased river discharge. Front. Mar. Sci. 6, 642.
van Emmerik, T., Van Klaveren, J., Meijer, L.J., Krooshof, J.W., Palmos, D.A.A., Tanchuling, M.A., 2020. Manila river mouths act as temporary sinks for macroplastic pollution. Front. Mar. Sci. 7, 770. https://doi.org/10.3389/fmars.2020.545812.
van Emmerik, T., Mellink, Y., Hauk, R., Waldschläger, K., Schreyers, L., 2022a. Rivers as plastic reservoirs. Front. Water 3, 1–8.
van Emmerik, T., de Lange, S., Frings, R., Schreyers, L., Aalderink, H., Leusink, J., Vriend, P., 2022b. Hydrology as a driver of floating river plastic transport. Earth's Future 10 (8), e2022EF002811.
Van Sebille, E., England, M.H., Froyland, G., 2012. Origin, dynamics and evolution of ocean garbage patches from observed surface drifters. Environ. Res. Lett. 7 (4), 044040.
Van Sebille, E., Griffies, S.M., Abernathey, R., Adams, T.P., Berloff, P., Biastoch, A., Zika, J.D., 2018. Lagrangian ocean analysis: fundamentals and practices. Ocean Model 121, 49–75.
Van Sebille, E., Aliani, S., Law, K.L., Maximenko, N., Alsina, J.M., Bagaev, A., Bergmann, M., Chapron, B., Chubarenko, I., Cózar, A., Delandmeter, P., 2020. The physical oceanography of the transport of floating marine debris. Environ. Res. Lett. 15 (2), 023003.
Vermeiren, P., Muñoz, C.C., Ikejima, K., 2016. Sources and sinks of plastic debris in estuaries: a conceptual model integrating biological, physical and chemical distribution mechanisms. Mar. Pollut. Bull. 113 (1–2), 7–16.
Warner, J.C., Geyer, W.R., Lerczak, J.A., 2005. Numerical modeling of an estuary: a comprehensive skill assessment. J. Geophys. Res. Oceans 110 (C5).
Wilcox, C., Van Sebille, E., Hardesty, B.D., 2015. Threat of plastic pollution to seabirds is global, pervasive, and increasing. Proc. Natl. Acad. Sci. 112 (38), 11899–11904.
Wilkin, J.L., Arango, H.G., Haidvogel, D.B., Lichtenwalner, C.S., Glenn, S.M., Hedström, K.S., 2005. A regional ocean modeling system for the Long-term Ecosystem Observatory. J. Geophys. Res. Oceans 110 (C6).
Williams, B.L., 1986. Flushing time calculations for the upper Waitemata Harbour, New Zealand. N. Z. J. Mar. Freshw. Res. 20 (3), 455–465.
Willmott, C.J., 1982. Some comments on the evaluation of model performance. Bull. Am. Meteorol. Soc. 63 (11), 1309–1313.
Yao, W., Di, D., Wang, Z., Liao, Z., Huang, H., Mei, K., Shang, X., 2019. Micro-and macroplastic accumulation in a newly formed Spartina alterniflora colonized estuarine saltmarsh in southeast China. Mar. Pollut. Bull. 149, 110636.
Young, M., Adams, N.J., 2010. Plastic debris and seabird presence in the Hauraki Gulf, New Zealand. N. Z. J. Mar. Freshw. Res. 44 (3), 167–175.
Zhang, H., 2017. Transport of microplastics in coastal seas. Estuar. Coast. Shelf Sci. 199, 74–86.